Superwetting Monolithic Hollow-Carbon-Nanotubes Aerogels with Hierarchically Nanoporous Structure for Efficient Solar Steam Generation

Peng Mu, Zheng Zhang, Wei Bai, Jingxian He, Hanxue Sun, Zhaoqi Zhu, Weidong Liang, and An Li*

Solar steam generation has been proven to be one of the most efficient approaches for harvesting solar energy for diverse applications such as distillation, desalination, and production of freshwater. Here, the synthesis of monolithic carbon aerogels by facile carbonization of conjugated microporous polymer nanotubes as efficient solar steam generators is reported. The monolithic carbon-aerogel networks consist of randomly aggregated hollow-carbon-nanotubes (HCNTs) with 100–250 nm in diameter and a length of up to several micrometers to form a hierarchically nanoporous network structure. Treatment of the HCNTs aerogels with an ammonium peroxydisulfate/sulfuric acid solution endows their superhydrophilic wettability which is beneficial for rapid transportation of water molecules. In combination with their abundant porosity (92%) with open channel structure, low apparent density (57 mg cm^{-3}), high specific surface area (826 m^2 g^{-1}), low thermal conductivity (0.192 W m^{-1} K^{-1}), and broad light absorption (99%), an exceptionally high conversion efficiency of 86.8% is achieved under 1 sun irradiation, showing great potential as an efficient photothermal material for solar steam generation. The findings may provide a new opportunity for tailored design and creation of new carbon-aerogels-based photothermal materials with adjustable structure, tunable porosity, simple fabrication process, and high solar energy conversion efficiency for solar steam generation.

Solar energy is a kind of renewable and theoretically inexhaustible energy, efficient harvesting, and utilization of solar energy has long been considered as a green and sustainable way for addressing severe issues worldwide such as energy crisis, environmental pollution, and global warming caused by the consumption of the fossil fuels.[1] Apart from diverse manners for utilization of solar energy such as production of

hydrogen,[2] solar power plants,[3] photovoltaic cells,[4] photocatalysis,[5] and water desalination,[6] the photothermal materials based solar water evaporation is one of the most promising approaches for harvesting and conversion of solar energy. Solar vapor generation, more specifically, is a surface water evaporation process in which the light is absorbed and converted to heat energy by photothermal materials to generate vapor. Compared with the common water evaporation by solar radiation as heat source which suffers from the drawback of low solar energy conversion efficiency due to the fact that the part solar energy is converted to heat bulk water or is lost to the external environment, solar vapor generation based on photothermal materials has great advantages for its high light-to-heat conversion efficiency due to the fact that solar radiation is only harvested and located at the water–air interface to heat thin air–water surface layer that can effectively minimize the heat loss.[7] Based on the merits mentioned above, up to now, the solar steam generator has been emerged as a kind of efficient device for harvesting solar energy and attracted extensively much more attention in both industrial and academic research throughout the past decades.[8,9]

In a given solar steam generation system, the photothermal materials is essential. A desired photothermal material should meet the following criteria: the broadband sunlight absorbability, low thermal conductivity, open porosity for rapid water molecules transportation, and high-energy conversion efficiency.[10,11] Understanding of these complementary roles of these parameters for photothermal material, so far, a number of photothermal materials, including carbon-based materials,[7,8,12–14] metallic nanoparticles,[15–17] biomass-based materials,[18,19] and porous polymers,[20,21] etc., have been developed to use as efficient solar steam generators.

In general, porous materials with bilayer structure are widely adapted as solar steam generator, in which the top layer consists of carbon materials for light absorption (e.g., graphene,[13] CNTs,[14] graphite,[7] etc.) while the bottom layer is composed by the porous materials (e.g., wood,[18] silica,[10] etc.) for

P. Mu, Z. Zhang, W. Bai, J. He, Dr. H. Sun, Dr. Z. Zhu, Prof. W. Liang, Prof. A. Li
Department of Chemical Engineering
College of Petrochemical Engineering
Lanzhou University of Technology
Lanzhou 730050, P. R. China
E-mail: lian2010@lut.cn

The ORCID identification number(s) for the author(s) of this article can be found under https://doi.org/10.1002/aenm.201802158.

**ADVANCED
SCIENCE NEWS**
www.advancedsciencenews.com

**ADVANCED
ENERGY
MATERIALS**
www.advenergymat.de

transportation of water molecules and preventing heat loss. The advantages for employment of those natural materials lie in their cost efficiency, environmentally friendliness, and high solar energy conversion efficiency. On the other hand, porous carbon materials especially carbon-based aerogels, owing to their highly porous feature, low thermal conductivity, and broad light absorption, show great potentials as photothermal materials for solar steam generation.[8] Comparatively, the intrinsic properties of carbon-based aerogels enable themselves as an integrated part that can serve as porous platform for harvesting light, transportation of water molecules, and preventing heat loss. For instance, graphene-based aerogels[22,23] were reported as standalone solar steam generator with a high-energy conversion efficiency of up to 83%. Great progress has been achieved in the past decade due to the unique characteristics of carbon-based aerogels and the current efforts on the design of carbon-based solar generators are to meet the criteria mentioned above. In fact, however, it is difficult to integrate all of the above features (criteria for photothermal materials) into one single-component material. In particular, the inherent fragility and poor mechanical strength of carbon-based aerogels dramatically limited their widespread applications. Therefore, the design and construction of a carbon-based aerogels with adjustable porosity, tunable structure, desired robustness, and practical processability still remain a big challenge.

As a kind of porous organic polymers, conjugated microporous polymers (CMPs) have attracted considerable attention due to their rigid π-conjugated structure, large specific surface areas, tunable porous structure, and good physical-co-chemical stability for a wide variety of applications.[24,25] Compared with traditional porous materials, the CMPs have great advantages for their designable flexibility and synthetic diversity for tailored-design CMPs-based porous materials for specific purpose.[26,27] More interestingly, the micromorphology and macrostructure of the CMPs precursor kept unchanged after pyrolysis treatment which makes it possible to control the porosity and macrostructure of the resultant CMPs-based product.[28,29] Based on these unique characteristics, it would be natural to assume that the CMPs should be ideal precursor as photothermal materials. Here, we report the synthesis of monolithic carbon aerogels by simple carbonization of CMPs for efficient solar steam generation. We also highlight that the surface modification of the resulting monolithic carbon aerogels makes them superhydrophilic which facilitate the rapid transportation of water molecules. In combination with their abundant porosity with open channel structure, low apparent density, high specific surface area, low thermal conductivity, and broad light absorption, an exceptionally high solar steam generation efficiency of up to 86.8% is achieved under 1 sun irradiation, which may hold great potentials as high-performance solar steam generators for solar steam generation.

As shown in **Figure 1**a, the conjugated microporous polymers aerogels (CMPAs) were synthesized by Sonogashira–Hagihara cross-coupling reaction of 1,3,5-triethynylbenzene with 1,4-dibromobenzene and 4,4′-dibromobiphenyl using Pd(0)/CuI as catalysts, triethylamine and toluene as co-solvents. After reaction, both CMPA-1 and CMPA-2 (Figure 1b,e) were prepared as yellow cylindrical monolithic materials with 3.0 cm in height and 3.2 cm in diameter. Figure 1c,f shows

the scanning electron microscope (SEM) images of the as-prepared conjugated microporous aerogels, in which both the CMPA-1 and CMPA-2 consist of the nanotubes roughly ranging from 100 to 250 nm in diameter. The transmission electron microscope (TEM) images further confirm the hollow tubular morphologies of the CMPA-1 and CMPA-2. As depicted in Figure 1d,g, the CMPA-1 possesses a rough surface, while the CMPA-2 shows relative neat external tubular surface with ≈50 nm in interior diameter.

The preparation of CMPs-based carbon aerogels was conducted by a simple carbonization of the as-formed carbon-rich tubular CMPs aerogels precursors to obtain conjugated microporous polymer carbon aerogels (CMPCAs). As shown in **Figure 2**a, the as-prepared CMPs aerogels were first sliced into rounds with 32 mm in diameter and 10 mm in height and then carbonized at 600 °C for 2 h with a heating rate of 2 °C min^{-1} under Ar atmosphere. After carbonization, the CMPs-based carbon aerogels retained its original shapes without any collapsing of its structures due to the 3D rigid carbon skeleton of CMP nanotubes. The apparent density was estimated to be 57 mg cm^{-3} for CMPCA-1 and 60 mg cm^{-3} for CMPCA-2 by dividing the weight by the volume, in which, the low apparent density makes CMPCAs stand on a dog's tail grass (Figure 2c). Besides, the as-prepared CMPCAs exhibit high mechanical property which can support a 500 g of weight without any collapsing of its original structure after removing the load (Figure 2d). Similar to previous study,[28,29] after carbonization, in this work, the microscopic morphologies of the resulting CMPs-based carbon aerogels remain unchanged, showing excellent physicochemical stability of the CMPs aerogels. Scanning electron microscopy (SEM) shows that CMPCA-1 and CMPCA-2 obtained from pyrolysis of CMPA-1 and CMPA-2, respectively, are mainly in form of rough surface nanotubes with a diameter of ≈100–250 nm and a length of up to several micrometers (Figure 2e,g). Transmission electron microscopy (TEM), as shown in Figure 2f,h, reveals that both CMPCA-1 and CMPCA-2 are formed with hollow nanotubes with 20–100 nm in interior diameter.

Powder X-ray diffraction pattern of CMPCAs show broad peak (Figure 2i), indicating the amorphous character of CMPCAs that is similar to the previously reported CMPs.[26] In the Raman spectra of CMPCA-1 and CMPCA-2 (shown in Figure 2j), two characteristic peaks around 1340 and 1590 cm^{-1} are observed, which are assigned to disordered (D-band) and ordered graphitic carbons (G-band),[30] respectively. The I_D/I_G ratio of CMPCA-1 is slight higher than that of the CMPCA-2, indicating a relative low graphitization of CMPCA-1 than that of CMPCA-2 after high-temperature pyrolysis. X-ray photoelectron spectroscopy (XPS), as shown in Figure 2k,l, shows sharp C 1s peak at ≈285.3 eV for CMPCA-1 and 286.8 eV for CMPCA-2, respectively. The presence of oxygen in both CMPCA-1 and CMPCA-2 can be ascribed to atmospheric O_2, H_2O, or CO_2 adsorbed onto the surface of CMPCAs.[31] The porosity of the CMPCAs was investigated by N_2 adsorption/desorption measurements performed at 77 K. As depicted in Figure 2m, both CMPCA-1 and CMPCA-2 display type I isotherms according to the IUPAC classification.[32] The steep adsorption increase in the low P/P_0 region (below 0.1) indicates the presence of micropores in the CMPCAs. The pore size distribution
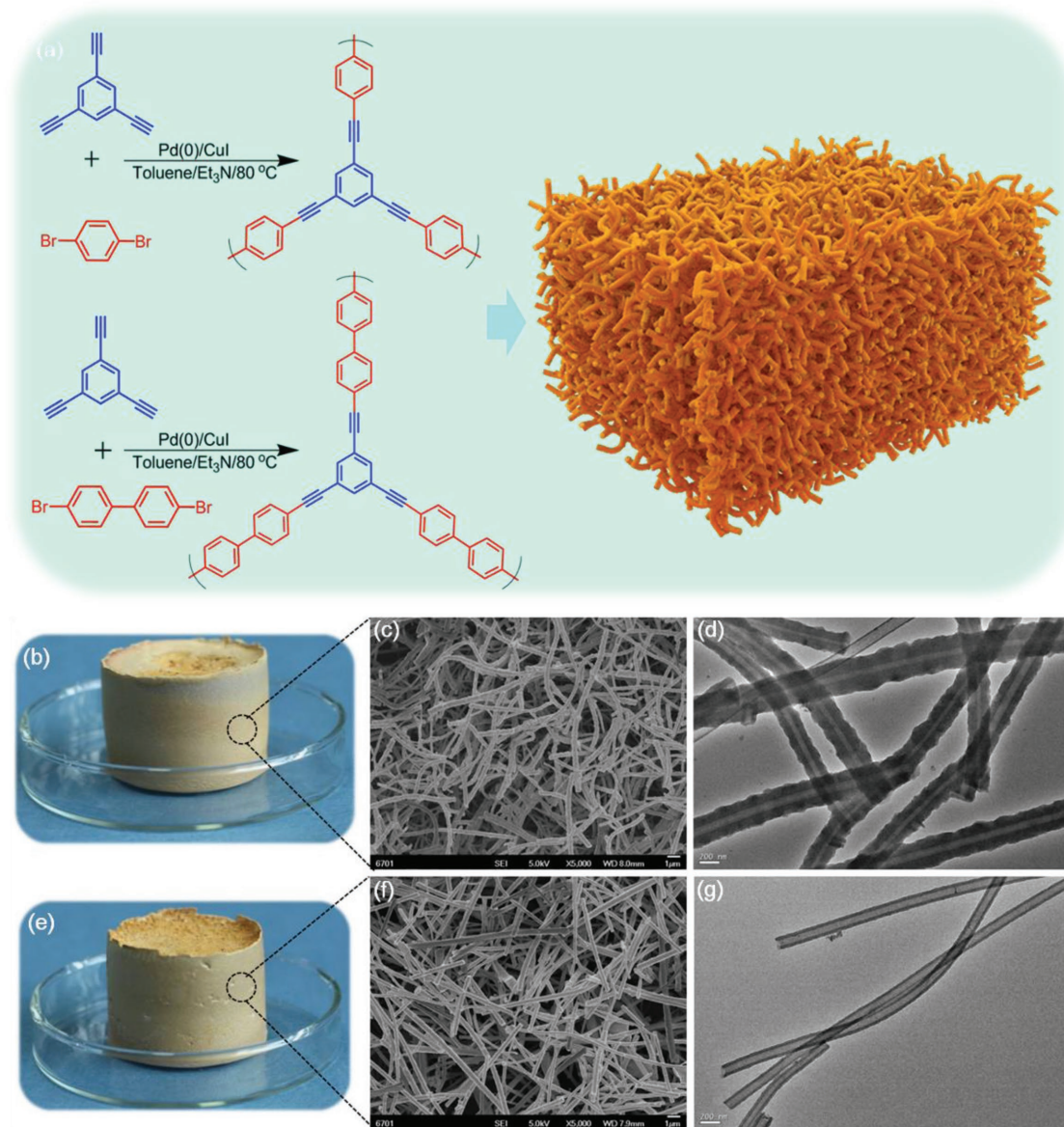
Figure 1. a) Synthesis of CMPs aerogels. b) Camera photo of CMPA-1. SEM images of c) CMPA-1, f) CMPA-2. e) Camera photo of CMPA-2. TEM images of d) CMPA-1, g) CMPA-2. Scale bar: c,f) 1 μm, d,g) 200 nm.

originated from the adsorption branches and calculated by applying Barrett–Joyner–Hallender (BJH) method is mainly concentrated in 1.93 nm for these two CMPs-based carbon aerogels (shown in Figure 2n). The specific surface areas calculated by Brunauer–Emmett–Teller (BET) model were found to be 826 m^2 g^{-1} for CMPCA-1 and 509 m^2 g^{-1} for CMPCA-2, respectively. The micropore area was calculated by using t-plot method to be 658 m^2 g^{-1} for CMPCA-1 and 422 m^2 g^{-1} for CMPCA-2, respectively. The pore volumes were calculated to be 0.62 cm^3 g^{-1} for CMPCA-1 and 0.33 cm^3 g^{-1} for CMPCA-2. The micropore volumes was found to be 0.34 cm^3 g^{-1} for CMPCA-1 and 0.22 cm^3 g^{-1} for CMPCA-2 by using t-plot method, respectively. Besides, the porosity of the CMPCAs measured by using liquid displacement procedure[33] was found to be 92.1% for CMPCA-1 and 91.7% for CMPCA-2, indicating excellent porous

feature of the CMPs-based carbon aerogels. Owing to their abundant porosity, the as-prepared CMPs-based carbon aerogels possess desired heat-insulated property. The thermal conductivity was measured to be 0.192 W m^{-1} K^{-1} for CMPCA-1 and 0.189 W m^{-1} K^{-1} for CMPCA-2 at room temperature by using flash method, respectively.

Due to the inherent carbon skeleton of the CMPAs, the as-prepared CMPCAs show hydrophobic surface which makes them hard to be fully wetted by the water, thus hindering the transportation of the water molecules. As shown in **Figure 3**a, the as-prepared CMPCA-1 floated on the water and could not be fully wetted by water within 2 min. To solve this, the resulting CMPs-based carbon aerogels were treated by the ammonium peroxydisulfate saturated 1 M H_2SO_4. As depicted in Figure 3b, after treatment, the CMPCA-1 shows superhydrophilic

**ADVANCED
SCIENCE NEWS**

www.advancedsciencenews.com
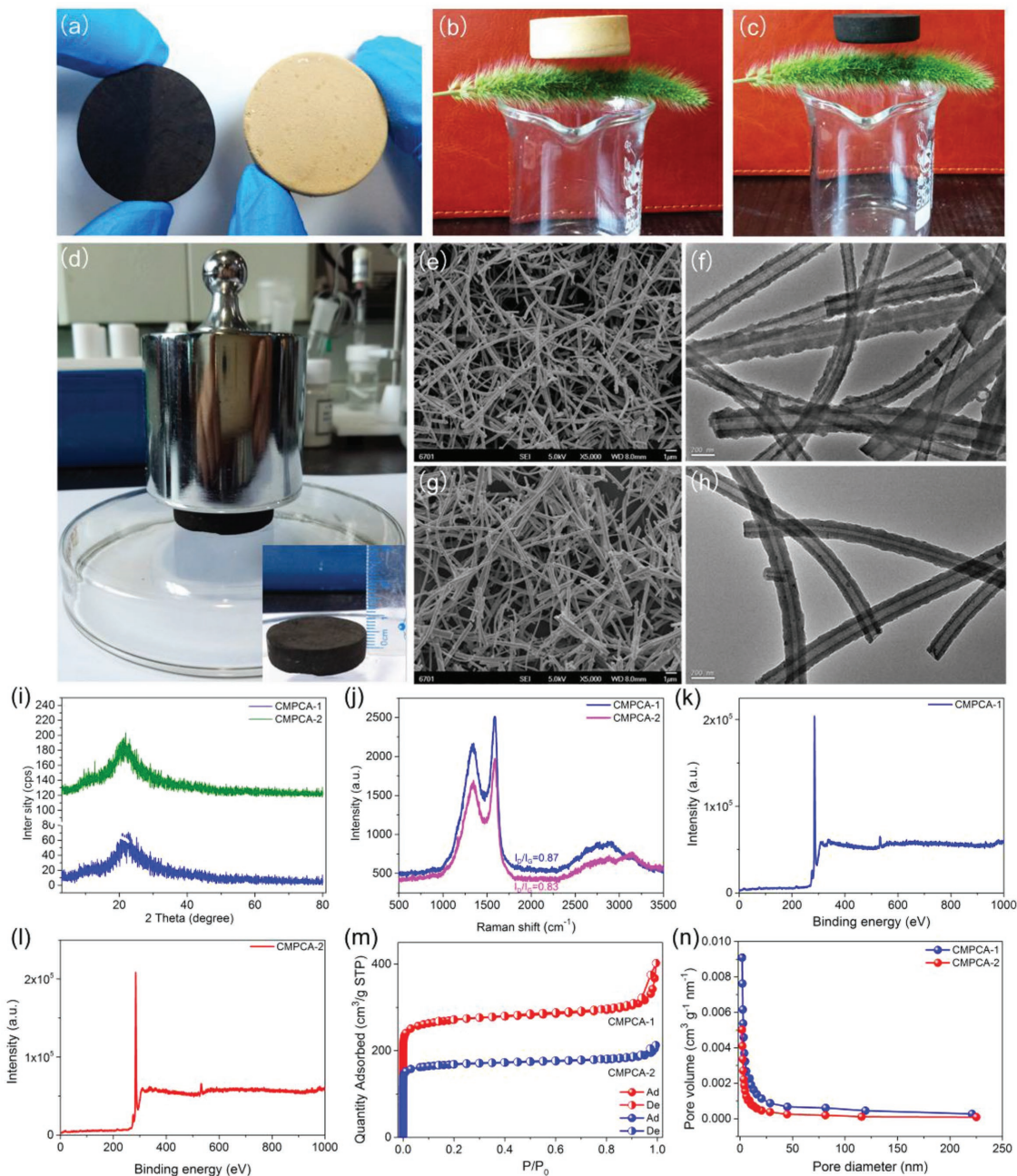
**ADVANCED
ENERGY
MATERIALS**

www.advenergymat.de

Figure 2. a) Camera photo of CMPCA-1 and CMPA-1. b) Camera photo of CMPA-1 on a dog's tail grass. c) Camera photo of CMPCA-1 on a dog's tail grass. d) Camera photo of CMPCA-1 under 500 g weight. Inset is the camera photo of CMPCA-1 after removing static load. SEM images of e) CMPCA-1 and g) CMPCA-2. TEM images of f) CMPCA-1 and h) CMPCA-2. Scale bar: e,g) 1 µm, f,h) 200 nm. i) XRD patterns of CMPCAs. j) Raman spectra of CMPCAs. k) XPS spectra of CMPCA-1. l) XPS spectra of CMPCA-2. m) N_2 adsorption/desorption isotherms of CMPCAs. n) Pore size distributions of the CMPCAs calculated by BJH method.

property and can be wetted by water within 20 s. To further confirm the wettability of the as-prepared CMPCA-1, the high-speed video camera was used to record the impregnation process and the results of camera photos are shown in Figure 3c,d. The impregnation process of the as-prepared CMCA-1 is very slow and the droplet cannot be fully impregnated within 50 s, while the CMPCA-1 treated by the ammonium peroxydisulfate saturated 1 M H_2SO_4 shows superhydrophilic property and can be wetted by water within 20 s. To further

the droplet can be fully impregnated with 6 s, indicating the excellent water transportation property. Most importantly, the modified CMPCAs can float on the water surface due to their porous structure and low density which is benefit to their solar steam generation performance. To further clarify the surface chemistry of the CMPCAs after treated by the ammonium peroxydisulfate saturated 1 M H_2SO_4, the XPS analysis was conducted and the results are illustrated in **Figure 4**a–d.

**ADVANCED
SCIENCE NEWS**
www.advancedsciencenews.com
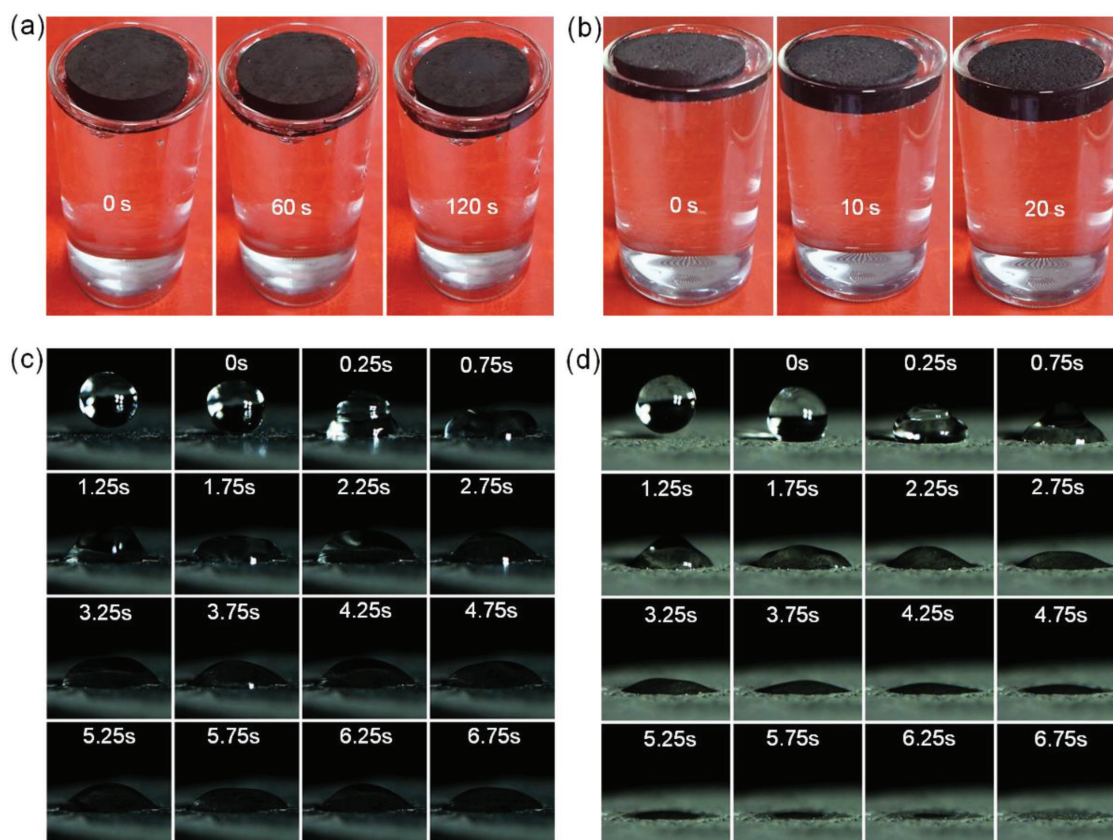
**ADVANCED
ENERGY
MATERIALS**
www.advenergymat.de

Figure 3. a) Camera photos of CMPCA-1 floating on the water surface. b) Camera photos of hydrophilic treated CMPCA-1 floating on the water surface. c) Camera photos of droplet impregnation process on the surface of CMPCA-1. d) Camera photos of droplet impregnation process on the surface of hydrophilic treated CMPCA-1.

After treatment with ammonium peroxydisulfate saturated 1 M H_2SO_4, the oxygen atomic concentration increased from 3.42% to 11.63% for CMPCA-1 and from 3.48% to 9.79% for CMPCA-2, respectively. The oxygen atomic concentration of the CMPCA-1 is relative higher than the CMPCA-2 may be attributed to its higher BET specific surface area than the CMPCA-2. The C1s spectra can be deconvoluted into four subpeaks that have been assigned to carbon in aromatic and aliphatic structures (284.7 eV); phenol, ether, or enol–keto groups (285.4 eV); carbonyl or quinone (287.1 eV); and carboxyl or ester groups (289.1 eV), respectively.[34] All of results indicate that after treated by the ammonium peroxydisulfate saturated 1 M H_2SO_4, the resulting CMPCAs possess oxygen-containing groups which makes the CMPCAs have superhydrophilic property, thus beneficial for the rapid transportation of the water molecules for solar steam generation.

The optical absorption of the CMPCAs was measured by UV–vis–NIR spectrometer (JASCO V-670) from 200 to 2500 nm with an integrated sphere. As shown in Figure 4e, both the CMPCA-1 and CMPCA-2 show almost 100% light absorption across 200–2500 nm due to the porous structure which facilitates the light absorption via multiple scattering of absorbed light.[35] Also, we have tested the optical reflectance of the CMPCAs and the results are illustrated in Figure S1 in the Supporting Information. From the Figure S1 in the Supporting Information, we can see clearly that both of the CMPCA-1 and

CMPCA-2 exhibit very low reflectance and the reflectance is less than 1%, indicating the excellent light absorption of the CMPCAs. Taking advantages of the porous nanotubes structure, superhydrophilic property, low thermal conductivity, and excellent optical absorption, the as-prepared CMPCAs should be a promising platform for solar steam generation. To confirm this, the water evaporation performance of the CMPCAs under different illuminations of 1, 2, and 3 kW m^{-2} was systematically investigated by using a labmade, real-time measurement system and the mass change of the water due to the steam generation was measured by an electronic analytical balance (Figure 4f). As shown in Figure 4g, under solar radiation of 1 and 2 kW m^{-2}, no obvious steam was observed, with further increasing of the solar radiation from 2 to 3 kW m^{-2}, the visible steam flow can be observed which is attributed to hot localized solar thermal conversion on the surface of the CMPCAs.

To confirm the solar energy conversion efficiency of the CMPCAs, the time-dependent mass change of the water due to steam generation was measured by the electronic analytical balance and the curves are illustrated in **Figure 5**a,b. From the Figure 5a,b, we can see clearly that the amount of water evaporated increased with the increasing of the solar radiation. The evaporation rates calculated from the slope of the time-dependent mass change curves were found to be 1.4406 kg m^{-2} h^{-1} under 1 kW m^{-2}, 2.796 kg m^{-2} h^{-1} under 2 kW m^{-2}, and 4.1778 kg m^{-2} h^{-1} under 3 kW m^{-2} for CMPCA-1-based solar
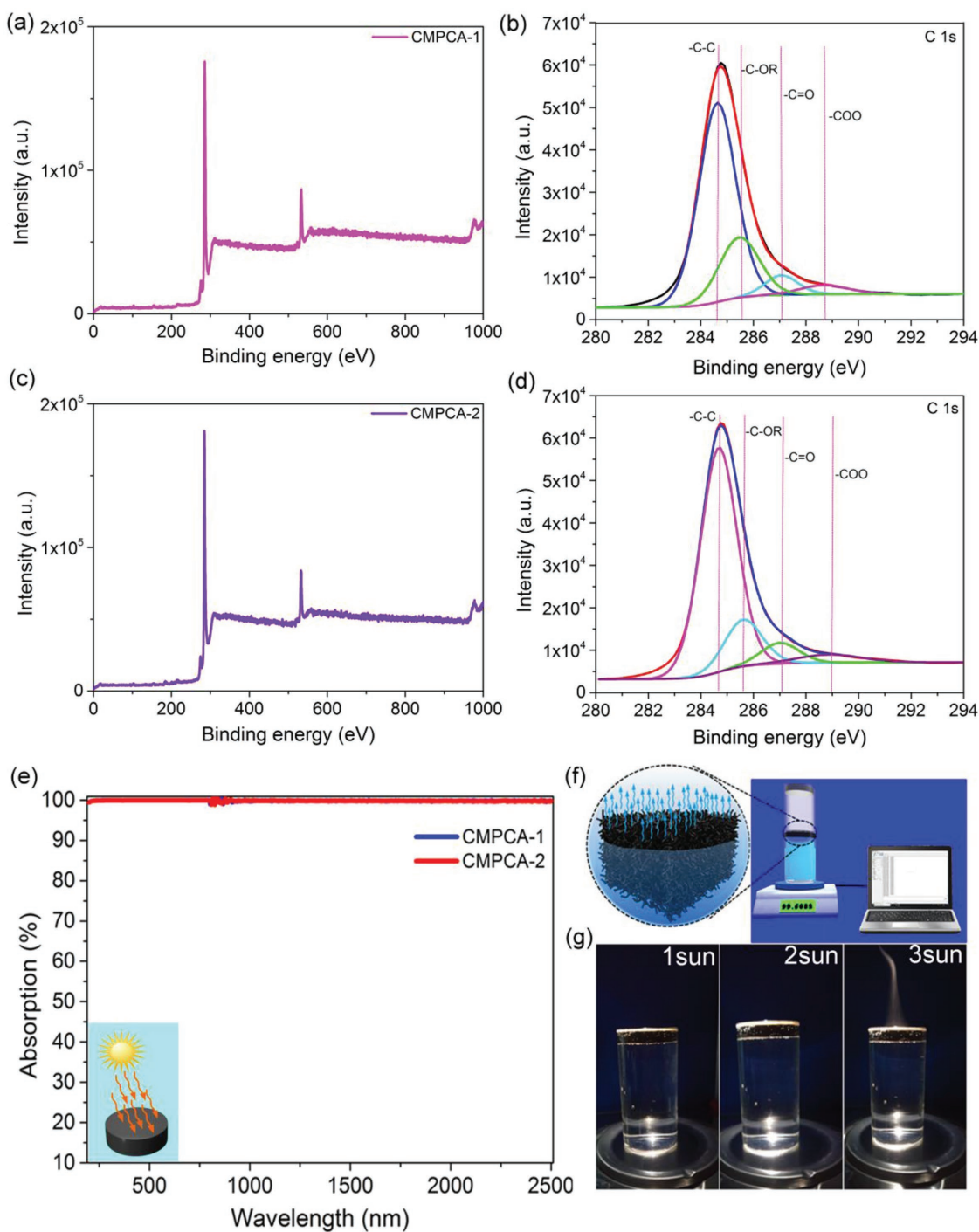
Figure 4. a) XPS spectra of CMPCA-1 after acid treatment. b) C1s XPS spectra of CMPCA-1 after acid treatment. c) XPS spectra of CMPCA-1 after acid treatment. d) C1s XPS spectra of CMPCA-2 after acid treatment. e) UV–vis–NIR absorption spectra of the CMPCAs. Inset is schematic diagram of solar energy absorption. f) Schematic of solar steam generation. g) Camera Photos of steam generated under varied solar irradiation energy of 1, 2, and 3 kW m^{-2} (1–3 sun).

receiver. As for CMPCA-2, the evaporation rates reached up to 1.3728 kg m^{-2} h^{-1} under 1 kW m^{-2}, 2.6112 kg m^{-2} h^{-1} under 2 kW m^{-2}, and 3.9186 kg m^{-2} h^{-1} under 3 kW m^{-2}, respectively. As control, the evaporation rates of pure water without CMPCAs was calculated to be 0.435 kg m^{-2} h^{-1} under 1 kW m^{-2} illumination whose value is much less than that of CMPCAs

under same illumination, indicating the efficient solar conversion performance of the CMPCAs. To further investigate heat localization caused by CMPs-based carbon aerogels under different solar intensities, infrared camera was used to monitor the surface temperature variations of the CMPCAs. As depicted in Figure 5c–f, the surface temperature increases from 21.7 to
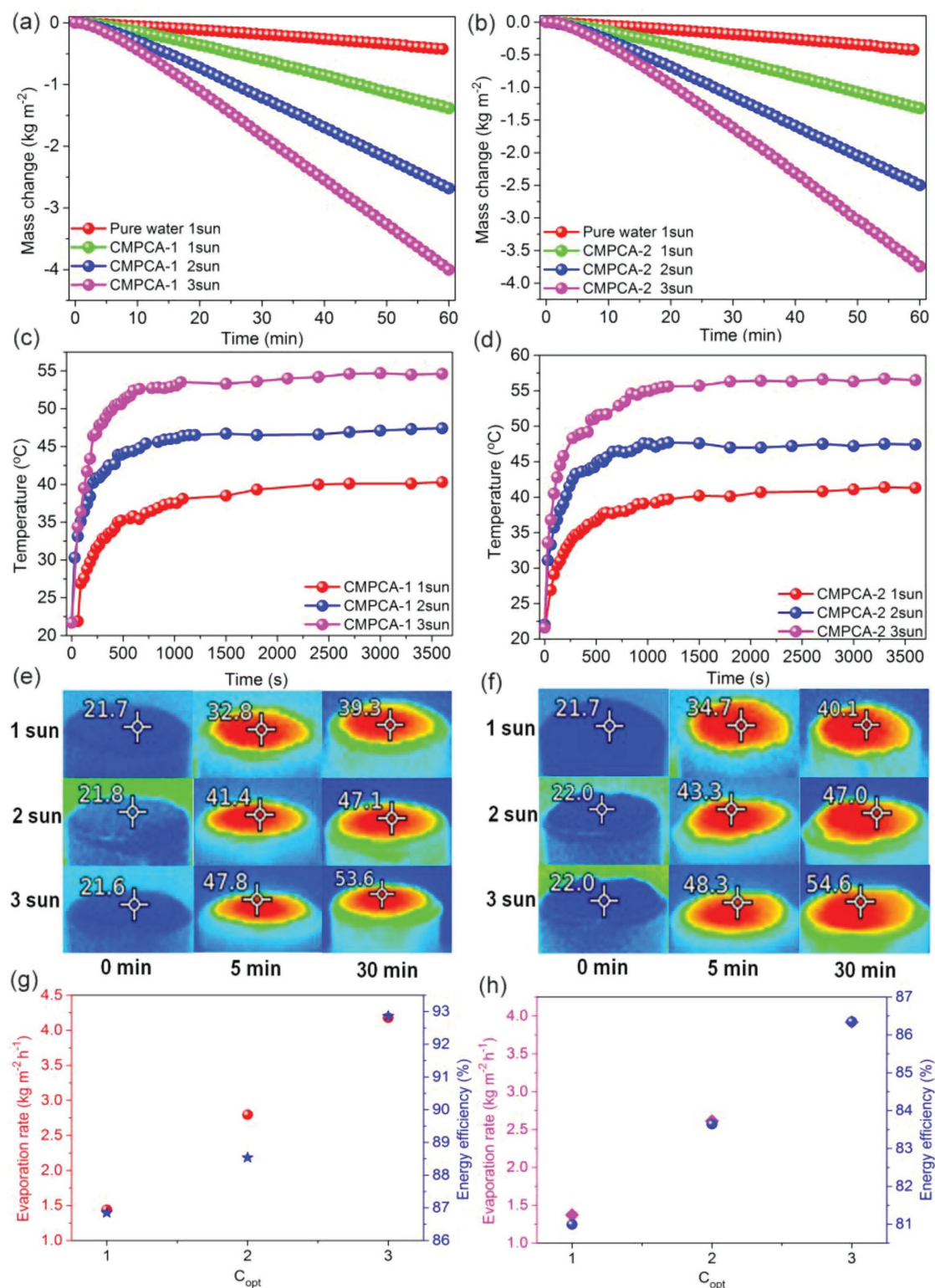
**ADVANCED
SCIENCE NEWS**

www.advancedsciencenews.com

**ADVANCED
ENERGY
MATERIALS**

www.advenergymat.de

Figure 5. a) Time-dependent mass change of the CMPCA-1 under different illuminations. b) Time-dependent mass change of the CMPCA-2 under different illuminations. c) Surface temperature change of CMPCA-1under different illuminations. d) Surface temperature change of CMPCA-2 under different illuminations. e) Infrared images of CMPCA-1 under different illuminations and time. f) Infrared images of CMPCA-2 under different illuminations and time. g) Evaporation rate (red, left-hand side axis) and solar steam efficiency (blue, right-hand side axis) of CMPCA-1 under different illuminations. h) Evaporation rate (pink, left-hand side axis) and solar steam efficiency (blue, right-hand side axis) of CMPCA-2 under different illuminations.

**ADVANCED
SCIENCE NEWS**
www.advancedsciencenews.com

**ADVANCED
ENERGY
MATERIALS**
www.advenergymat.de

37.5 °C under 1 kW m^{-2} illumination, 46 °C under 2 kW m^{-2} illumination, and 53.1 °C under 3 kW m^{-2} illumination within 1000 s, and then further to 40.5 °C under 1 kW m^{-2} illumination, 47.4 °C under 2 kW m^{-2} illumination, and 54.6 °C under 3 kW m^{-2} illumination within 1 h, respectively, for CMPCA-1. These values go from 39.2 °C at power density of 1 kW m^{-2}, 47.5 °C at power density of 2 kW m^{-2}, and 55 °C at power density of 3 kW m^{-2} in the first 1000 s and then further increases to 41.3, 47.4, and 56.5 °C at power density of 1, 2, and 3 kW m^{-2} within 1 h, respectively, for CMPCA-2, indicating excellent solar energy conversion efficiency performance of the CMPCAs. The energy conversion efficiency was calculated according to the literature[36] and the detailed calculation was present in Supporting Information. The energy conversion efficiency of the pure water without CMPCAs was calculated to be 21.3% under at power density of 1 kW m^{-2} which is much less than that of the CMPCA-1 and CMPCA-2 under same solar intensity. The energy conversion efficiency was found to be 86.8% for CMPCA-1 and 81% for CMPCA-2, respectively, under 1 kW m^{-2} illumination, which are much higher than that of the previous reported solar steam generation devices.[20,37,38] It is noted that the CMPCA-1 shows relative higher energy conversion efficiency than that of the CMPCA-2, which may be attributed to the relative higher BET specific surface area and micropore volume of CMPCA-1 than CMPCA-2 where it provides more channels for the rapid transportation of water molecules by hierarchically porous structure combining with capillary action of micropores.

In summary, we have demonstrated the synthesis of hollow-carbon-nanotubes (HCNTs) aerogels for efficient solar steam generation. The HCNTs aerogels derived from pyrolysis of CMP nanotubes possess abundant porosity (92%) with super-hydrophilic open channel structure, low apparent density (57 mg cm^{-3}), broad light absorption (99%), and low thermal conductivity (0.192 W m^{-1} k^{-1}) all of which characteristics endow the resulting CMPCAs with rapid water transportation, self-floating property, excellent light-to-heat conversion, and thermal heat insulation performance, thus an exceptionally high solar steam generation efficiency of up to 86.8% is achieved under 1 sun irradiation. The findings of this work may provide a new opportunity for tailored-design and creating new carbon-aerogel-based photothermal materials with adjustable structure, tunable porosity, simple fabrication process, and high solar energy conversion efficiency for solar steam generation.

Experimental Section

Chemicals: 1,3,5-Triethynylbenzene was obtained from TCI. 1,4-Dibromobenzene, 4,4′-Dibromobiphenyl, tetrakis(triphenylphosphine)palladium(0), and Copper (I) iodide were purchased from J&K-Chemical Co., Ltd. Toluene, Et$_3$N, and others were obtained from Tianjin Fuyu chemical reagent Co., Ltd. and used as received without further purification.

Synthesis of the CMPs Aerogels: The CMPAs were synthesized by Sonogashira-Hagihara cross-coupling reaction of 1,3,5-triethynylbenzene with 1,4-dibromobenzene and 4,4′-dibromobiphenyl using Pd(0)/CuI as catalyst. The molar ratio of ethynyl to bromo functionalities in the monomer feed was set at 2:1.

CMP Aerogels-1: 1,3,5-Triethynylbenzene(600.72 mg 4 mmol), 1,4-dibromobenzene (707.7 mg 3 mmol), CuI (100 mg), and tetrakis-(triphenylphosphine)palladium(0) (200 mg) were first added into a flat-bottom glass test tube. After degassed for 20 min, 15 mL of toluene and 15 mL of Et$_3$N were added into the glass test tube by using an injection syringe, respectively. The mixture was degassed again for 20 min and then stirred with magnetic stirring until the temperature reached up to 80 °C. The reaction system continued to react for 72 h under 80 °C without stirring. After complete reaction, the product was naturally cooled to the room temperature and the raw product was filtered and washed with chloroform, acetone, water, and methanol for several times to remove any unreacted monomers or catalyst residues. The CMPAs was then further purified by Soxhlet extraction (methanol) for 3 d and dried at 70 °C for 24 h to get a constant weight. Elemental combustion analysis (%) Calcd for C$_{21}$H$_9$: C 96.55, H 3.45; found: C 75.85, H 3.46.

CMP Aerogels-2: For CMPA-2, 1,3,5-triethynylbenzene(600.72 mg 4 mmol) and 4,4′-dibromobiphenyl (936 mg 3 mmol) were used as monomers. C$_{30}$H$_{15}$: C 96.0, H 4.0; found: C 78.22, H 3.57.

Preparation of CMPs-Based Carbon Aerogels: The CMPs aerogels-1 (CMPA-1) wafer with 3.2 cm in diameter and 1 cm in height was placed into a porcelain boat and heated up to 600 °C for 2 h with a heating rate of 2.0 °C min^{-1} under argon atmosphere. The product was treated in acetone, water, and ethanol respectively, to remove impurities under stirring for 4 h. The resulting sample was dried at 70 °C for 24 h to obtain a constant weight and named as CMPs carbon aerogels-1 (CMPCA-1).

The preparation of CMPs carbon aerogels-2 was obtained as same as CMPCA-1 just using CMPA-2 as precursor and the product was named as CMPCA-2.

Supporting Information

Supporting Information is available from the Wiley Online Library or from the author.

Conflict of Interest

The authors declare no conflict of interest.

[1] N. L. Panwar, S. C. Kaushik, S. Kothari, *Renewable Sustainable Energy Rev.* **2011**, *15*, 1513.
[2] M. R. Shaner, H. A. Atwater, N. S. Lewis, E. W. McFarland, *Energy Environ. Sci.* **2016**, *9*, 2354.

**ADVANCED
SCIENCE NEWS**

www.advancedsciencenews.com

**ADVANCED
ENERGY
MATERIALS**

www.advenergymat.de

[3] J. Khan, M. H. Arsalan, *Renewable Sustainable Energy Rev.* **2016**, *55*, 414.

[4] L. Ye, X. Jiao, M. Zhou, S. Zhang, H. Yao, W. Zhao, A. Xia, H. Ade, J. Hou, *Adv. Mater.* **2015**, *27*, 6046.

[5] J. Fei, J. Li, *Adv. Mater.* **2015**, *27*, 314.

[6] C. M, A. Yadav, *Renewable Sustainable Energy Rev.* **2017**, *67*, 1308.

[7] H. Ghasemi, G. Ni, A. M. Marconnet, J. Loomis, S. Yerci, N. Miljkovic, G. Chen, *Nat. Commun.* **2014**, *5*, 4449.

[8] V.-D. Dao, H.-S. Choi, *Global Challenges* **2018**, *2*, 1700094.

[9] L. Zhu, M. Gao, C. K. N. Peh, G. W. Ho, *Mater. Horiz.* **2018**, *5*, 323.

[10] Y. Wang, L. Zhang, P. Wang, *ACS Sustainable Chem. Eng.* **2016**, *4*, 1223.

[11] Y. Li, T. Gao, Z. Yang, C. Chen, W. Luo, J. Song, E. Hitz, C. Jia, Y. Zhou, B. Liu, B. Yang, L. Hu, *Adv. Mater.* **2017**, *29*, 1700981.

[12] L. Zhu, M. Gao, N. Peh Connor Kang, X. Wang, W. Ho Ghim, *Adv. Energy Mater.* **2018**, *8*, 1702149.

[13] P. Zhang, J. Li, L. Lv, Y. Zhao, L. Qu, *ACS Nano* **2017**, *11*, 5087.

[14] Z. Yin, H. Wang, M. Jian, Y. Li, K. Xia, M. Zhang, C. Wang, Q. Wang, M. Ma, Q.-S. Zheng, Y. Zhang, *ACS Appl. Mater. Interfaces* **2017**, *9*, 28596.

[15] M. Zhu, Y. Li, F. Chen, X. Zhu, J. Dai, Y. Li, Z. Yang, X. Yan, J. Song, Y. Wang, E. Hitz, W. Luo, M. Lu, B. Yang, L. Hu, *Adv. Energy Mater.* **2018**, *8*, 1701028.

[16] L. Zhou, Y. Tan, D. Ji, B. Zhu, P. Zhang, J. Xu, Q. Gan, Z. Yu, J. Zhu, *Sci. Adv.* **2016**, *2*, e1501227.

[17] K. Bae, G. Kang, S. K. Cho, W. Park, K. Kim, W. J. Padilla, *Nat. Commun.* **2015**, *6*, 10103.

[18] T. Li, H. Liu, X. Zhao, G. Chen, J. Dai, G. Pastel, C. Jia, C. Chen, E. Hitz, D. Siddhartha, R. Yang, L. Hu, *Adv. Funct. Mater.* **2018**, *28*, 1707134.

[19] K.-K. Liu, Q. Jiang, S. Tadepalli, R. Raliya, P. Biswas, R. R. Naik, S. Singamaneni, *ACS Appl. Mater. Interfaces* **2017**, *9*, 7675.

[20] L. Zhang, B. Tang, J. Wu, R. Li, P. Wang, *Adv. Mater.* **2015**, *27*, 4889.

[21] Q. Chen, Z. Pei, Y. Xu, Z. Li, Y. Yang, Y. Wei, Y. Ji, *Chem. Sci.* **2018**, *9*, 623.

[22] X. Hu, W. Xu, L. Zhou, Y. Tan, Y. Wang, S. Zhu, J. Zhu, *Adv. Mater.* **2017**, *29*, 1604031.

[23] Y. Fu, G. Wang, T. Mei, J. Li, J. Wang, X. Wang, *ACS Sustainable Chem. Eng.* **2017**, *5*, 4665.

[24] I. Cooper Andrew, *Adv. Mater.* **2009**, *21*, 1291.

[25] Y. Xu, S. Jin, H. Xu, A. Nagai, D. Jiang, *Chem. Soc. Rev.* **2013**, *42*, 8012.

[26] J.-X. Jiang, F. Su, A. Trewin, D. Wood Colin, L. Campbell Neil, H. Niu, C. Dickinson, Y. Ganin Alexey, J. Rosseinsky Matthew, Z. Khimyak Yaroslav, I. Cooper Andrew, *Angew. Chem., Int. Ed.* **2007**, *46*, 8574.

[27] R. Dawson, A. Laybourn, Y. Z. Khimyak, D. J. Adams, A. I. Cooper, *Macromolecules* **2010**, *43*, 8524.

[28] X. Feng, Y. Liang, L. Zhi, A. Thomas, D. Wu, I. Lieberwirth, U. Kolb, K. Müllen, *Adv. Funct. Mater.* **2009**, *19*, 2125.

[29] Q. Zhang, Q. Dai, M. Li, X. Wang, A. Li, *J. Mater. Chem. A* **2016**, *4*, 19132.

[30] K. Yuan, T. Hu, Y. Xu, R. Graf, L. Shi, M. Forster, T. Pichler, T. Riedl, Y. Chen, U. Scherf, *Mater. Chem. Front.* **2017**, *1*, 278.

[31] Z.-S. Wu, L. Chen, J. Liu, K. Parvez, H. Liang, J. Shu, H. Sachdev, R. Graf, X. Feng, K. Müllen, *Adv. Mater.* **2014**, *26*, 1450.

[32] M. Thommes, K. Kaneko, A. V. Neimark, J. P. Olivier, F. Rodriguez-Reinoso, J. Rouquerol, K. S. W. Sing, *Pure Appl. Chem.* **2015**, *87*, 1051.

[33] E. Kolanthai, P. A. Sindu, D. K. Khajuria, S. C. Veerla, D. Kuppuswamy, L. H. Catalani, D. R. Mahapatra, *ACS Appl. Mater. Interfaces* **2018**, *10*, 12441.

[34] P. Valle-Vigón, M. Sevilla, A. B. Fuertes, *Microporous Mesoporous Mater.* **2013**, *176*, 78.

[35] K. Kim, S. Yu, C. An, S.-W. Kim, J.-H. Jang, *ACS Appl. Mater. Interfaces* **2018**, *10*, 15602.

[36] S. Hong, Y. Shi, R. Li, C. Zhang, Y. Jin, P. Wang, *ACS Appl. Mater. Interfaces* **2018**, *10*, 28517.

[37] W. Xu, X. Hu, S. Zhuang, Y. Wang, X. Li, L. Zhou, S. Zhu, J. Zhu, *Adv. Energy Mater.* **2018**, *8*, 1702884.

[38] G. Xue, K. Liu, Q. Chen, P. Yang, J. Li, T. Ding, J. Duan, B. Qi, J. Zhou, *ACS App. Mater. Interfaces* **2017**, *9*, 15052.